Scripta Materialia 203 (2021) 114069

Contents lists available at ScienceDirect

Scripta Materialia

journal homepage: www.elsevier.com/locate/scriptamat

Exploring the hydrogen absorption and strengthening behavior in nanocrystalline face-centered cubic high-entropy alloys

Yakai Zhao[a,1,*], Jeong-Min Park[b,1], Kotaro Murakami[c], Shin-ichi Komazaki[c], Megumi Kawasaki[d], Koichi Tsuchiya[e], Jin-Yoo Suh[f], Upadrasta Ramamurty[a,g], Jae-il Jang[b,*]

[a] School of Mechanical and Aerospace Engineering, Nanyang Technological University, Singapore 639798, Republic of Singapore
[b] Division of Materials Science and Engineering, Hanyang University, Seoul 04763, Republic of Korea
[c] Department of Mechanical Engineering, Kagoshima University, Kagoshima 890-0065, Japan
[d] School of Mechanical, Industrial and Manufacturing Engineering, Oregon State University, Corvallis, OR 97331, U.S.A
[e] International Center for Young Scientists, National Institute for Materials Science (NIMS), Tsukuba, Ibaraki 305-0047, Japan
[f] Center for Energy Materials Research, Korea Institute of Science and Technology, Seoul 02792, Republic of Korea
[g] Institute of Materials Research Engineering, Agency for Science, Technology and Research, Singapore 138634, Republic of Singapore

ARTICLE INFO

Article history:
Received 6 May 2021
Revised 6 June 2021
Accepted 6 June 2021
Available online 19 June 2021

Keywords:
High-entropy alloy
Nanocrystalline
Hydrogen
Nanoindentation
Activation volume

ABSTRACT

The effect of marked change in grain size from coarse-grained to nanocrystalline can affect the hydrogen absorption and plastic deformation behavior in two face-centered cubic high-entropy alloys (HEAs), viz. equiatomic CoCrFeNi and CoCrFeMnNi. Thermal desorption analysis of the hydrogen-charged samples proved that grain boundaries act as hydrogen traps and thus largely increase the hydrogen contents in the nanocrystalline samples. A direct comparison in the hydrogen absorption between two HEAs confirms that both chemical composition and grain size are crucial factors contributing to the hydrogen solubility of the HEAs. The parameters for the thermally activated deformation from nanoindentation rate-jump tests suggest enhanced lattice friction by hydrogen, leading to a reduction in activation volume and thus modification of the plastic deformation processes. The results are discussed in two aspects, viz. the effect of grain size and chemical composition on the hydrogen-affected plastic deformation.

Among a wide variety of high-entropy alloys (HEAs), scientific investigations on the face-centered cubic (fcc) HEAs, which mostly consist of 3d transition elements, are the most extensive to date [1–3]. In addition to their prominent mechanical behavior [2,4,5], the performance that makes the HEAs a more interesting and practically valuable member of novel structural materials is their low susceptibility (and thus excellent resistance) to hydrogen embrittlement compared to conventional fcc metals and alloys [6–10]. Despite the research activities on the topic, one of the crucial issues unexplored yet is the following: “can the interesting hydrogen-related behavior be maintained in the highly strengthened fcc HEAs?” To date, a major theme of the research activities on fcc HEAs is strength enhancement in the relatively low yield strength at room temperature and a variety of avenues are explored [2,11–14]. While strengthening mechanisms for an alloy are mostly based on the interplay between dislocations and crystalline defects, the defects are also the sites extensively interacting with hydrogen (i.e., for hydrogen diffusion and trapping). Thus, higher fraction of defects may possibly lead to not only higher strength but, at the same time, higher susceptibility (viz. lower resistance) to hydrogen embrittlement, as reported for high-strength steels [15,16]. The former is beneficial for the wider application of HEAs, whereas the latter is detrimental. Therefore, with the application viewpoint, exploring this possible trade-off is very important.

An intriguing step aimed at this issue is to explore the hydrogen uptake and its effects in the fcc HEAs having very different fractions of defects. Grain boundary (GB) is a representative example of the defects controllable in an easy and obvious manner. While the grain size effect in the order of μm has been very recently studied [17,18], a more critical case of nanocrystalline (NC) fcc HEAs, whose microstructure and mechanical behavior are substantially different from those of the course-grained (CG) counterparts [19,20], have not been explored yet. Keeping this in view, we compare the hydrogen uptake and its effects on the relative hardness enhancements in NC and CG samples of two typical fcc HEAs in this study.

* Corresponding authors.
E-mail addresses: yakai.zhao@ntu.edu.sg (Y. Zhao), jijang@hanyang.ac.kr (J.-i. Jang).
[1] These authors contributed equally to this work.

https://doi.org/10.1016/j.scriptamat.2021.114069
1359-6462/

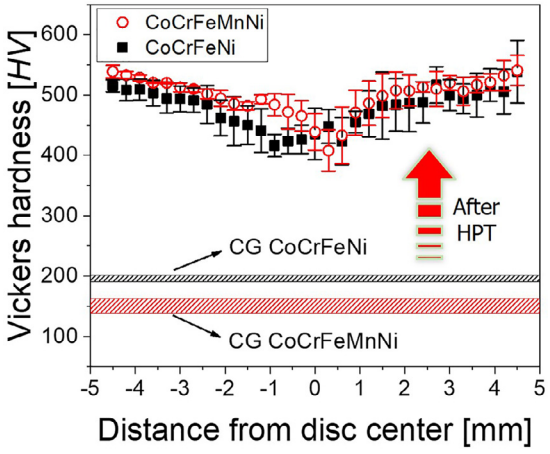

Fig. 1. Variations in Vickers hardness with distance from the center of the HPT-processed discs.

Two widely studied fcc HEAs with the nominal compositions (in at.%) of $Co_{25}Cr_{25}Fe_{25}Ni_{25}$ and $Co_{20}Cr_{20}Fe_{20}Mn_{20}Ni_{20}$ (referred to as CoCrFeNi and CoCrFeMnNi here after) were examined. They were synthesized by vacuum induction melting of pure metals. The ingots were then hot-rolled, homogenized (at 1000 and 1100°C, respectively) for 1 h, and water-quenched to obtain well-annealed CG samples. Discs with 10 mm diameter and ~0.83 mm thickness were machined from homogenized samples, and then subjected to HPT with an applied pressure of 5 GPa for 2 turns at 1 rpm. All the specimens were polished to a mirror finish (using 0.05 μm colloidal silica in the final step). Vickers hardness (*HV*) was measured with a peak load, P_{max}, of 980 mN. Microstructures of the specimens were examined using scanning electron microscopy (SEM; Verious G4 XHR, Thermo Fisher Scientific, Waltham, MA, USA) and transmission electron microscopy (TEM Talos F200X, Thermo Fisher Scientific, Waltham, MA, USA). For TEM, a thin electron-transparent layer was milled and lifted by focused ion beam (FIB; Nova 200 NanoLab, FEI, Hillsboro, OR, USA) from the vertical cross-sections at the edges of the HPT-processed discs.

The polished specimens were electrochemically hydrogen charged [21,22] at room temperature (RT, ~25°C) with a potentiostat/galvanostat equipment with a current density of 100 mA/cm^2 for 24 h in an electrolyte containing 0.1 mol/L NaOH and 0.5 wt.% NH_4SCN. All the subsequent experiments were conducted right after charging. Thermal desorption spectroscopy (TDS) was performed using a gas chromatograph (JTF-20A, J-Science Lab, Kyoto, Japan) at a constant heating rate of 100 °C/h. Nanoindentation experiments were conducted on CG specimens and at the edges of each HPT specimen using a Nanoindenter-XP (KLA, Milpitas, CA, USA) with a Berkovich tip. The nanohardness (*HN*) measurements were performed at constant indentation strain rate of $\dot{\varepsilon}$ (= (d*h*/d*t*)/*h*, where *h* is depth and *t* is time) of 0.025 s^{-1} with P_{max} = 100 mN. Additionally, strain-rate jump tests were performed to a maximum depth of 2500 nm with $\dot{\varepsilon}$ ranging from 0.0005 to 0.025 s^{-1}. (See Fig. S1 in the Supplementary Information (SI) for details.).

Variations of *HV* along diameters of the HPT discs of the two HEAs are shown in Fig. 1. For comparison, *HV* of the CG samples before HPT are also displayed. As expected, a substantial hardness enhancement due to HPT, across the entire disc diameters, is observed. A gradual increase in *HV* with the distance from the center, *r*, of HPT disks is also seen. Since the imposed strain increases with *r* during HPT, the microstructural refinement is substantial in the peripheral regions [13,19,23]. The *HV* values at the disc edges are ~2.8 to 3.6 times *HV* of CG CoCrFeNi and CoCrFeMnNi, respectively.

Representative microstructures of the CG and NC HEAs are displayed in Fig. 2. The backscattered electron (BSE) images of CG samples in Figs. 2a and 2e show well annealed microstructures consisting of coarse grains (with *d* of ~28 and ~61 μm for CoCrFeNi and CoCrFeMnNi, respectively) and some annealing twins. Bright-field TEM images (Figs. 2b and 2f) obtained from the edge regions of the HPT specimens reveal marked grain refinement; estimated *d* values are ~46 and ~45 nm for CoCrFeNi and CoCrFeMnNi, respectively. The combined effect of the significant enhancement in atomic diffusivity during the HPT process [13] and relatively low stacking fault energy (SFE) [19,24] in the fcc HEAs (~26.8 and ~17 mJ/m^2 for CoCrFeNi and CoCrFeMnNi, respectively [25]) are the reasons for the ready nanocrystallization during HPT. Thus, the significant hardening observed in the peripheral regions of the HPT samples is mainly due to grain refinement as the Hall-Petch coefficient of HEAs is substantially larger compared to that of conventional fcc metals and alloys [13,19,26]. An increase in the dislocation and deformation twin densities could be additional contributors to the observed strengthening [19,27,28].

The selected area electron diffraction (SAED) patterns (Figs. 2c and 2g) reveal single-phase fcc structure in both the alloys. Together with the X-ray diffraction results (Fig. S2 in SI), they confirm that no phase transformation takes place during HPT. The energy dispersive X-ray spectroscopy (EDS) maps obtained during TEM (Figs. 2d and 2h) indicate homogeneous distributions of constituent elements without any noticeable segregation or clustering in both the samples.

In Fig. 3, *HN* of the hydrogenated NC and CG samples are compared with those of their uncharged counterparts. An increase in HN upon hydrogen charging is noted in all cases. Importantly, the percentage increase in HN is much smaller in both NC HEAs (~7%) whereas it is substantial in CG samples (~57% for CoCrFeMnNi and ~29% for CoCrFeNi). The estimated values of the Hall-Petch coefficient, k_{HP}, in both HEAs with and without hydrogen (Fig. S3 in SI) suggest that hydrogenation does not affect the grain boundary's strengthening ability in a significant manner.

To gain more insights into the influence of hydrogen on the plastic deformation mechanisms of HEAs, we performed nanoindentation strain-rate jump tests for estimating the rate-dependent, thermally-activated deformation parameters, viz. the strain rate sensitivity *m* and the activation volume V^*. Since the rate jump tests can substantially reduce experimental time compared to multiple constant strain rate tests [29,30], they offers a great advantage in effectively reducing the potential influence of hydrogen outgassing on the obtained results. In order to account for the indentation size effect [31], *HN* right before and after each transient $\dot{\varepsilon}$ change at specific depths (*h* = 1000, 1500, and 2000 nm) are used for estimating *m* and V^* [30] according to

$$m = \frac{\partial \ln H}{\partial \ln \dot{\varepsilon}} = \frac{\ln H_2 - \ln H_1}{\ln \dot{\varepsilon}_2 - \ln \dot{\varepsilon}_1}, \quad (1)$$

where the subscripts '1' and '2' denote the *HN* values obtained before and after the transient $\dot{\varepsilon}$ change, respectively, and

$$V^* = \sqrt{3} kT \frac{\partial \ln \dot{\varepsilon}_1}{\partial (H/C)} = \sqrt{3} kTC \frac{\ln \dot{\varepsilon}_2 - \ln \dot{\varepsilon}_1}{H_2 - H_1} \quad (2)$$

where *k* is the Boltzmann's constant, *T* is the temperature, and *C* is the constraint factor [13]. The average values of *m* and V^* estimated using the above equations for the two HEAs with CG and NC microstructures are displayed in Fig. 4a and 4b, respectively. While both grain refinement and hydrogen charging increase *m*, they reduce V^*.

The thermal desorption spectra obtained on different samples are displayed in Fig. 5. The hydrogen contents in the charged CG samples are ~4.3 and ~24.7 wppm for CoCrFeNi and CoCrFeMnNi, respectively. It is significantly higher in the charged NC samples

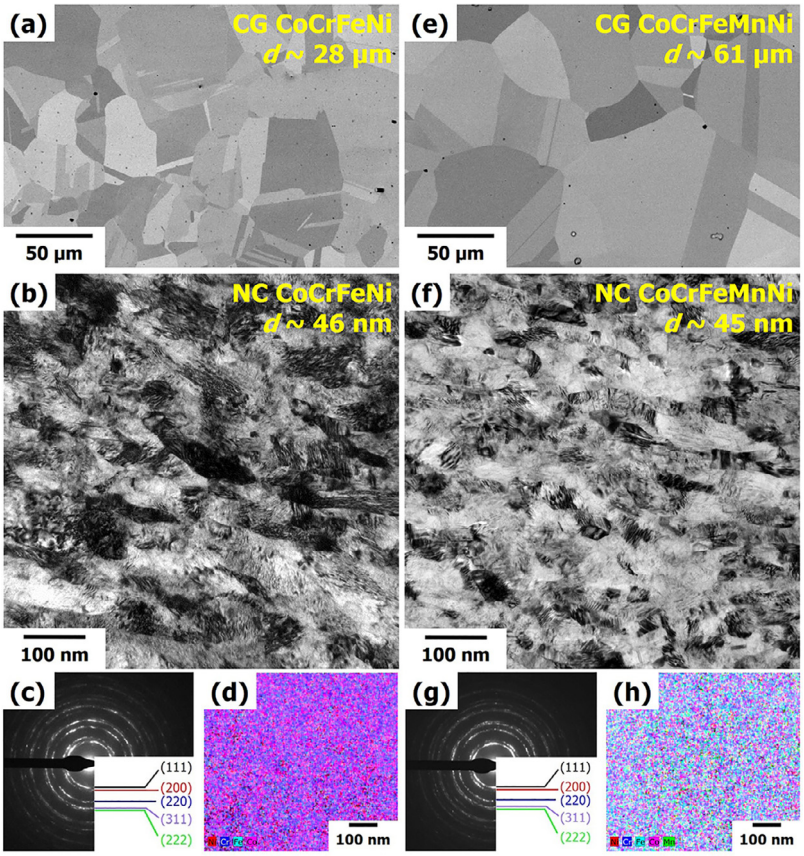

Fig. 2. Typical microstructure of the (a–d) CoCrFeNi and (e–h) CoCrFeMnNi HEAs: (a,e), SEM BSE images; (b,f), TEM bright field images; (c,g) TEM SAED patterns, (d,h) TEM EDS maps.

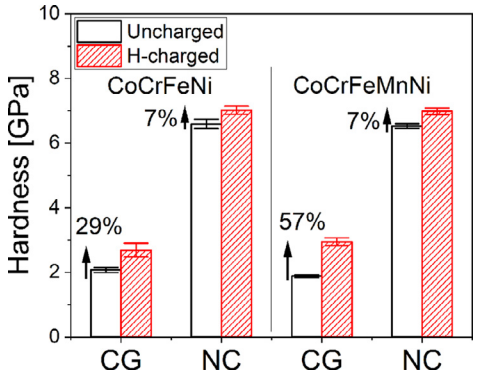

Fig. 3. Hardness changes caused by hydrogen charging in CoCrFeNi and CoCrFeMnNi HEAs. The given percentage is for the normalized hardness increment by hydrogen charging.

(45.6 and 90.8 wppm), with it being nearly-double in the CoCrFeMnNi HEA than in the CoCrFeNi HEA.

The influence of chemical composition and grain size of the alloy are utilized below to discuss the results obtained.

(1) *Chemical composition:* The relatively higher hydrogen uptake in CoCrFeMnNi HEA, irrespective of *d*, implies that the hydrogen's solubility in it is much higher than in CoCrFeNi under identical charging conditions [32]. This observation appears to be consistent with the data reported in the literature, as summarized in Table 1 [8,9,17,18,33], and confirm that hydrogen solubility is sensitive to the chemical composition of the alloy. While the precise reasons responsible for such high hydrogen solubility in

Table 1
Comparison of the hydrogen contents (in wppm) in CoCrFeNi and CoCrFeMnNi HEAs under exactly same hydrogen charging conditions in various grain size regimes. Coarse-grained alloys represent those with grain sizes of >10 μm, while fine-grained is for 1 to 10 μm, and nanocrystalline is for <100 nm [32].

Grain size regime	CoCrFeNi	CoCrFeMnNi	References
Coarse-grained	4.3	24.7	Present study
	54.3	113.0	Koyama *et al.* [17,33]
	58.5	146.9	Nygren *et al.* [8,9]
Fine-grained	63.7	129.0	Koyama *et al.* [17,18]
Nanocrystalline	45.6	90.8	Present study

CoCrFeMnNi HEA are not known yet, the following ones have been suggested. (i) Severe lattice distortion associated with the large solute concentrations and the resulting high lattice strain energy may make the interstitial sites in HEAs more amenable for hydrogen atoms' residence [6,34]. However, this possibility can be ruled out on the basis of the present set of results, as the lattice distortion levels in the two HEAs are comparable [35,36] or the distortion is even slightly severer in CoCrFeNi [37,38] depending on the applied models or measures. (ii) In austenitic stainless steels (ASS), which are often compared with the CoCrFeMnNi HEA due to the similarity in the major alloying elements and fcc crystal structure [1,6,22], high Cr and Mn contents are known to enhance the hydrogen solubility [39]. In comparison to 316L ASS, which generally has 16–18 wt.% Cr and 2 wt.% Mn, CoCrFeNi has higher Cr content (nominally 23.2 wt.%) but no Mn, whereas CoCrFeMnNi possesses slightly higher Cr (18.6 wt.%) and substantially higher Mn content (19.6 wt.%) [6]. Such relative differences in the Cr and Mn contents

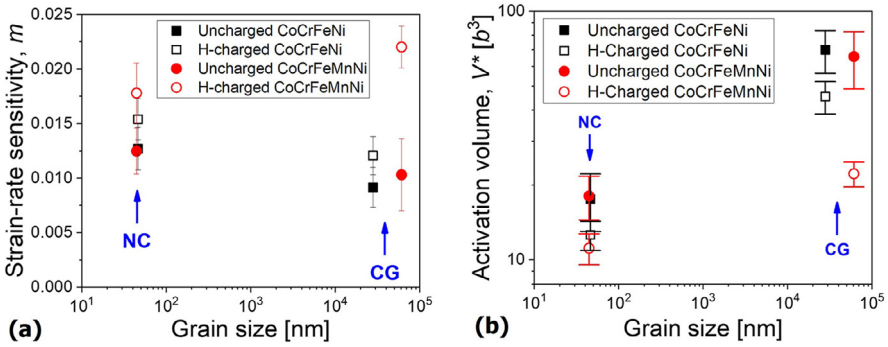

Fig. 4. (a) Strain-rate sensitivity and (c) activation volume values of CoCrFeNi and CoCrFeMnNi HEAs in both uncharged and hydrogen-charged states.

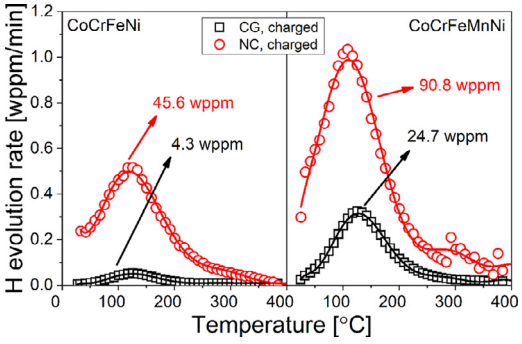

Fig. 5. TDS results of hydrogen-charged CoCrFeNi and CoCrFeMnNi HEAs.

can satisfactorily explain the observed H absorption differences among the two HEAs and 316L ASS. Koyama *et al.* [18] found that reducing Mn content from 20 to 13 at.% in Co-Cr-Fe-Mn-Ni HEAs can lead to a ~40% reduction in the absorbed content. (iii) Both experiments [40,41] and simulations [42] suggest that HEAs are heterogeneous at the nanoscale with the existence of the short-ranger ordered (SRO) domains, i.e., HEAs are not completely random solid solutions at the atomic scale. While such SRO domains may be suitable sites for higher hydrogen solubility, it is doubtful if CoCrFeMnNi would contain a remarkably higher level of SRO than CoCrFeNi.

(2) *Grain size*: Compared to CG samples, the hydrogen-induced hardening in the NC samples is much smaller. They also exhibit smaller V^* values despite having significantly higher hydrogen contents. Opposing trends in the hydrogen-induced hardness enhancement and absorbed hydrogen contents are seen, i.e., higher the hydrogen content in the alloy, smaller is the increase in *HN* upon charging. This suggest that the hydrogen content in the alloy may not necessarily dominate the hydrogen sensitivity of material properties, at least in terms of strength/hardness. For ductility/toughness, we speculate that hydrogen may also exert a lesser influence on the NC HEAs; as such, the low ductility of NC alloys [43] may further marginalize the hydrogen effects. Insights into the possible reasons can be gained by analyzing the predominant deformation mechanisms inferred through the V^* values in terms of b^3 (where b is the magnitude of Burgers vector). In fcc metals, V^* varies by orders of magnitude for different rate-limiting processes, with typical values of $>$ ~$100b^3$ for dislocation forest cutting, ~$10b^3$ for GB sliding, and ~$1b^3$ to ~$10b^3$ for diffusion either along GBs or through the crystalline lattice [44,45]. As noted from Fig. 4b, V^* in the NC samples varies between ~11 and $18b^3$, whereas V^* of the CG samples ranges between ~22 and $70b^3$. The latter values are in good agreement with our previous study [19]. A V^* of ~$10b^3$ in NC HEAs suggests that their deformation mechanisms are consistent with conventional NC metals, i.e. GB-mediated dislocation activity (dislocation nucleation and/or dislocation depinning at GBs [44,46]). On the contrary, CG HEAs show lower V^* values than those in conventional CG metals ($>$ ~$100b^3$ [44]), suggesting that the short-range barriers, which are responsible for thermally activated deformation process [45,47], are enhanced. This is because HEAs possess much higher lattice friction stress, (i.e., much stronger Peierls barrier to dislocation motion) than pure or dilute fcc metals and alloys [48,49], leading to the reduction in V^* of CG HEAs [48–50].

Values of V^* obtained on hydrogen-charged samples are always lower than those of the uncharged ones, indicating an increase in the lattice friction stress for dislocation motion caused by the absorbed hydrogen. This is consistent with the results reported on CoCrFeMnNi HEA [51] that show increased lattice friction with the charging time (and hence increased hydrogen content in the alloy). Such an enhancement in the friction stress reduces the dislocation mobility, and in turn, increases hardness with a concomitant decrease in V^*, which ultimately can enhance the ability of hydrogen to embrittle the alloy. Such a contribution, however, would be minor in NC samples [52,53] since GBs plays the predominant role in strengthening, as evidenced from the above analysis on V^*; this explains the relatively lower hydrogen-induced hardening in the NC samples. It is noteworthy that the exceptionally low V^* in the hydrogen-charged CG CoCrFeMnNi HEA may be related with the high hydrogen solubility in it (nearly 6 times that measured in hydrogen-charged CG CoCrFeNi) [54].

In summary, the coupled roles of grain size and chemical composition on the relative influence of hydrogen on the hardening of CoCrFeNi and CoCrFeMnNi HEAs were investigated. Results suggest that the grain boundaries in HEAs increase the hydrogen absorption substantially. The relative strengthening due to hydrogen in fine grained alloys is much smaller. A comparison of CoCrFeNi and CoCrFeMnNi HEAs suggests that the alloy's chemical composition, rather than the 'randomness' in composition (or chemical SRO), dictates the extent of hydrogen uptake during charging, with Cr and Mn being the key elements. The constitutive parameters for rate-dependent, thermally-activated deformation processes, estimated using the nanoindentation rate-jump tests, indicate that hydrogen reduces the lattice friction stress in HEAs and thus modifies the underlying mechanisms governing the plastic deformation.

The work at Hanyang University was supported by the National Research Foundation of Korea (NRF) grants funded by the Korea government (MSIT) (No. 2020R1A2B5B01001446 and No. 2020R1A5A6017701). The work at Nanyang Technological University was supported by the funding from A*STAR via the Structural Metals and Alloys Programme (No. A18B1b0061). The work at Kagoshima University was supported by JSPS KAKENHI grant number 21K04694 (Grant-in-Aid for Scientific Research (C)). The work at Oregon State University was supported by the National

Science Foundation (NSF) of the United States (No. DMR-1810343). The work at NIMS was supported by a Grant-in-Aid for Scientific Research on Innovative Area, "High-Entropy Alloys-Science of New Class of Materials Based on Elemental Multiplicity and Heterogeneity" through MEXT, Japan (contract no. 18H05451). The authors thank Liang Li and Zhe Gao for helping experiments.

Declaration of Competing Interest

The authors declare that they have no known competing financial interests or personal relationships that could have appeared to influence the work reported in this paper.

Supplementary materials

Supplementary material associated with this article can be found, in the online version, at doi:10.1016/j.scriptamat.2021.114069.

References

[1] D.B. Miracle, O.N. Senkov, Acta Mater 122 (2017) 448–511.
[2] Z. Li, S. Zhao, R.O. Ritchie, M.A. Meyers, Prog. Mater. Sci. 102 (2019) 296–345.
[3] K. Biswas, J.-W. Yeh, P.P. Bhattacharjee, J.T.M. DeHosson, Scr. Mater. 188 (2020) 54–58.
[4] B. Gludovatz, A. Hohenwarter, D. Catoor, E.H. Chang, E.P. George, R.O. Ritchie, Science (80-.) 345 (2014) 1153–1158.
[5] B. Gludovatz, A. Hohenwarter, K.V.S. Thurston, H. Bei, Z. Wu, E.P. George, R.O. Ritchie, Nat. Commun. 7 (2016) 1–8.
[6] Y. Zhao, D.-H. Lee, M.-Y. Seok, J.-A. Lee, M.P. Phaniraj, J.-Y. Suh, H.-Y. Ha, J.-Y. Kim, U. Ramamurty, J. Jang, Scr. Mater. 135 (2017) 54–58.
[7] G. Yang, Y. Zhao, D.-H. Lee, J.-M. Park, M.-Y. Seok, J.-Y. Suh, U. Ramamurty, J. Jang, Scr. Mater. 161 (2019) 23–27.
[8] K.E. Nygren, S. Wang, K.M. Bertsch, H. Bei, A. Nagao, I.M. Robertson, Acta Mater 157 (2018) 218–227.
[9] K.E. Nygren, K.M. Bertsch, S. Wang, H. Bei, A. Nagao, I.M. Robertson, Curr. Opin. Solid State Mater. Sci. 22 (2018) 1–7.
[10] C.K. Soundararajan, H. Luo, D. Raabe, Z. Li, Corros. Sci. 167 (2020) 108510.
[11] I. Basu, J.T.M. De Hosson, Scr. Mater. 187 (2020) 148–156.
[12] Z. Li, K.G. Pradeep, Y. Deng, D. Raabe, C.C. Tasan, Nature 534 (2016) 227–230.
[13] D.-H. Lee, I.-C. Choi, M.-Y. Seok, J. He, Z. Lu, J.-Y. Suh, M. Kawasaki, T.G. Langdon, J. Jang, J. Mater. Res. 30 (2015) 2804–2815.
[14] J.C. Rao, H.Y. Diao, V. Ocelík, D. Vainchtein, C. Zhang, C. Kuo, Z. Tang, W. Guo, J.D. Poplawsky, Y. Zhou, P.K. Liaw, J.T.M. De Hosson, Acta Mater 131 (2017) 206–220.
[15] M. Koyama, E. Akiyama, Y.-K. Lee, D. Raabe, K. Tsuzaki, Int. J. Hydrogen Energy 42 (2017) 12706–12723.
[16] M. Dadfarnia, A. Nagao, S. Wang, M.L. Martin, B.P. Somerday, P. Sofronis, Int. J. Fract. 196 (2015) 223–243.
[17] M. Koyama, K. Ichii, K. Tsuzaki, Int. J. Hydrogen Energy 44 (2019) 17163–17167.
[18] M. Koyama, H. Wang, V.K. Verma, K. Tsuzaki, E. Akiyama, Metall. Mater. Trans. A 51 (2020) 5612–5616.
[19] Y. Zhao, X. Wang, T. Cao, J.-K. Han, M. Kawasaki, J. Jang, H.N. Han, U. Ramamurty, L. Wang, Y. Xue, Mater. Sci. Eng. A 782 (2020) 139281, doi:10.1016/j.msea.2020.139281.
[20] D.H. Lee, M.Y. Seok, Y. Zhao, I.C. Choi, J. He, Z. Lu, J.Y. Suh, U. Ramamurty, M. Kawasaki, T.G. Langdon, J. Il Jang, Acta Mater 109 (2016) 314–322.
[21] Y. Zhao, M.-Y. Seok, I.-C. Choi, Y.-H. Lee, S.-J. Park, U. Ramamurty, J.-Y. Suh, J. Jang, Scr. Mater. 107 (2015) 46–49.
[22] Y. Zhao, J.-M. Park, D.-H. Lee, E.J. Song, J.-Y. Suh, U. Ramamurty, J. Jang, Scr. Mater. 168 (2019) 76–80.
[23] A.P. Zhilyaev, T.G. Langdon, Prog. Mater. Sci. 53 (2008) 893–979.
[24] Y.H. Zhao, X.Z. Liao, Y.T. Zhu, Z. Horita, T.G. Langdon, Mater. Sci. Eng. A 410–411 (2005) 188–193.
[25] A.J. Zaddach, R.O. Scattergood, C.C. Koch, Mater. Sci. Eng. A 636 (2015) 373–378.
[26] W.H. Liu, Y. Wu, J.Y. He, T.G. Nieh, Z.P. Lu, Scr. Mater. 68 (2013) 526–529.
[27] A. Heczel, M. Kawasaki, J.L. Lábár, J. Jang, T.G. Langdon, J. Gubicza, J. Alloys Compd. 711 (2017) 143–154.
[28] J. Gubicza, P.T.P.T. Hung, M. Kawasaki, J.J.-K. Han, Y. Zhao, Y. Xue, J.L.J.L. Lábár, Mater. Charact. 154 (2019) 304–314.
[29] V. Maier, K. Durst, J. Mueller, B. Backes, H.W. Höppel, M. Göken, J. Mater. Res. 26 (2011) 1421–1430.
[30] V. Maier, C. Schunk, M. Göken, K. Durst, Philos. Mag. 95 (2015) 1766–1779.
[31] W.D. Nix, H. Gao, J. Mech. Phys. Solids 46 (1998) 411–425.
[32] I.-C. Choi, J. Jang, Adv. Eng. Mater. 22 (2020) 1900648, doi:10.1002/adem.201900648.
[33] K. Ichii, M. Koyama, C.C. Tasan, K. Tsuzaki, Scr. Mater. 150 (2018) 74–77.
[34] Y. Zhao, D.-H. Lee, W.-J. Kim, M.-Y. Seok, J.-Y. Kim, H.N. Han, J.-Y. Suh, U. Ramamurty, J. Jang, Mater. Sci. Eng. A 718 (2018) 43–47.
[35] H. Song, F. Tian, Q.-M. Hu, L. Vitos, Y. Wang, J. Shen, N. Chen, Phys. Rev. Mater. 1 (2017) 023404.
[36] S. Yoshida, T. Ikeuchi, T. Bhattacharjee, Y. Bai, A. Shibata, N. Tsuji, Acta Mater 171 (2019) 201–215.
[37] N.L. Okamoto, K. Yuge, K. Tanaka, H. Inui, E.P. George, AIP Adv 6 (2016) 125008.
[38] L. Li, Q. Fang, J. Li, B. Liu, Y. Liu, P.K. Liaw, Mater. Sci. Eng. A 784 (2020) 139323.
[39] C. San Marchi, B.P. Somerday, S.L. Robinson, Int. J. Hydrogen Energy 32 (2007) 100–116.
[40] R. Zhang, S. Zhao, J. Ding, Y. Chong, T. Jia, C. Ophus, M. Asta, R.O. Ritchie, A.M. Minor, Nature 581 (2020) 283–287.
[41] Y. Zhao, J.-M. Park, J. Jang, U. Ramamurty, Acta Mater 202 (2021) 124–134.
[42] Q.J. Li, H. Sheng, E. Ma, Nat. Commun. 10 (2019) 1–11.
[43] B. Schuh, F. Mendez-Martin, B. Völker, E.P. George, H. Clemens, R. Pippan, A. Hohenwarter, Acta Mater 96 (2015) 258–268.
[44] Y.M. Wang, A.V. Hamza, E. Ma, Acta Mater 54 (2006) 2715–2726.
[45] D. Caillard, J.L. Martin, Thermally Activated Mechanisms in Crystal Plasticity, Pergamon, Amsterdam, 2003.
[46] C.D. Gu, J.S. Lian, Q. Jiang, W.T. Zheng, J. Phys. D. Appl. Phys. 40 (2007) 7440–7446.
[47] S. Gangireddy, B. Gwalani, R.S. Mishra, Mater. Sci. Eng. A 736 (2018) 344–348.
[48] Z. Wu, Y. Gao, H. Bei, Acta Mater 120 (2016) 108–119.
[49] J. Moon, S.I. Hong, J.B. Seol, J.W. Bae, J.M. Park, H.S. Kim, Mater. Res. Lett. 7 (2019) 503–509.
[50] M. Komarasamy, N. Kumar, R.S. Mishra, P.K. Liaw, Mater. Sci. Eng. A 654 (2016) 256–263.
[51] D. Wang, X. Lu, Y. Deng, D. Wan, Z. Li, A. Barnoush, Intermetallics 114 (2019) 106605.
[52] D.H. Lee, J.A. Lee, M.Y. Seok, U.B. Baek, S.H. Nahm, J. Il Jang, Int. J. Hydrogen Energy 39 (2014) 1897–1902.
[53] A. Barnoush, M. Asgari, R. Johnsen, Scr. Mater. 66 (2012) 414–417.
[54] Y. Zhao, M.-Y. Seok, D.-H. Lee, J.-A. Lee, J.-Y. Suh, J. Jang, Philos. Mag. 96 (2016) 3442–3450.